7.4 SIMULATION OF INERTIAL INSTABILITY IN A PRIMITIVE EQUATIONS MODEL

D. Pendlebury* and T. J. Dunkerton
NorthWest Research Associates, Inc., Bellevue, Washington

1 INTRODUCTION

Inertial instability may occur in a fluid when the angular momentum increases away from the axis of rotation. In the tropical middle atmosphere, this occurs when the maximum of the absolute angular momentum $\bar{M} = \Omega a \cos^2\varphi + \bar{u}\cos\varphi$ is located off the equator, due to a nonzero meridional shear in $\bar{u}$ at the equator. This is equivalent to the condition that

$$f\left(f - \frac{1}{a\cos\varphi}\frac{\partial}{\partial\varphi}(\bar{u}\cos\varphi)\right) \approx f(f - \bar{u}_y) < 0 \qquad (1)$$

somewhere, leading to equatorial inertial instability (EQII). EQII acts to rearrange $\bar{M}$ such that the maximum is located at the equator and $\bar{M}$ is conserved.

The linear, zonally symmetric theory predicts that EQII will generate overturning cells in the meridional wind $\bar{v}$ with corresponding temperature anomalies. In the absence of dissipation, these cells will develop at the smallest allowable vertical scale (Dunkerton 1981; Dunkerton 1993; Clark and Haynes 1996). In models the vertical wavelength of EQII will be $\lambda_z \sim 2\Delta z$, where Δz is the vertical resolution of the model (O'Sullivan and Hitchman 1992). The nonlinear response is similar however, the vertical wavelength is deeper (Griffiths 2003). Structures associated with EQII have also been noted in observations (Hayashi et al. 1998), with vertical wavelengths that are better explained by the nonlinear theory of EQII, although there are still many unanswered questions about what exactly these structures mean.

This paper will present the zonal structure of EQII in a 3d primitive equations model, showing that the instability has a zonal wavenumber(s) selected by the winter-hemispheric planetary waves which impinge upon the zero-wind line. The instability also generates smaller scale travelling waves which appear to be gravity waves. The dispersion relation of these waves will be examined.

2 MODEL RESULTS

2.1 Model Setup

The model solves the primitive equations for a dry, rotating, spherical atmosphere (Andrews et al. 1987) and uses a horizontal spectral truncation of T42. The vertical discretization uses 100 pressure levels spaced almost equally in log-pressure height with a resolution of approximately 670 m in the interior of the model and a lower boundary at 100 mb and upper boundary at 0.1 mb. Sampling of fields occurs every 3 hours.

Dissipation in the model is included in the form of ∇^8 hyperdiffusion and a second order vertical viscosity which act only on the deviation from the initial background state. Newtonian cooling relaxes the potential temperature back to the initial potential temperature. A nonzonal Rayleigh sponge layer is used above 70 km in order to dissipate waves in this region and prevent reflection off the upper boundary.

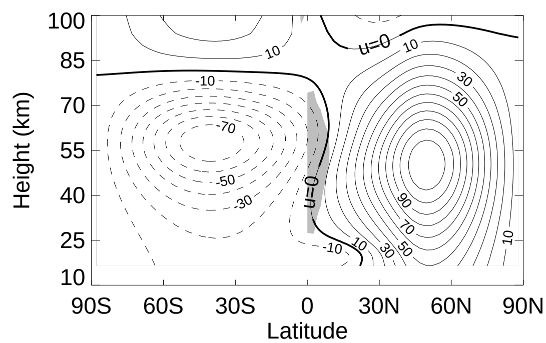

Figure 1: Initial zonal wind profile. Contour intervals are $10\,\mathrm{m\,s^{-1}}$. The $\bar{u} = 0$ line is indicated and the inertially unstable region in the tropics is shaded.

The initial conditions are set such that the background wind is similar to a northern hemisphere winter solstice conditions (Figure 1). The background vertical (globally averaged) stratification is chosen to be isothermal with a scale height of $H = 7$km which yields a buoyancy frequency of $N = 2 \times 10^{-2}\mathrm{s}^{-1}$. The initial winds are purely zonal ($\bar{v} = \bar{w} = 0$) and $\bar{u}$ is initially unstable to EQII, indicated by the shaded region in Figure 1. Stationary planetary waves are generated at the lower boundary by specifying the geopotential. The critical line for the forced waves is indicated in Figure 1 by the thick line denoted $\bar{u} = 0$, and passes through the region of EQII.

2.2 Role of winter planetary wave breaking

Stationary planetary waves with zonal wavenumbers 1 and 2 were used since these are the dominant waves in the wintertime stratosphere. The results shown are those for a forced planetary wave with zonal wavenumber 2 only. The planetary waves propagate into the stratosphere and towards the tropics where they encounter their critical line ($\bar{u} = 0$). The region of inertial instability is initially zonally symmetric, however, when the

*Corresponding author address: D. Pendlebury, NorthWest Research Associates, Inc., Bellevue, Washington, USA, 98007; e-mail: dpendle@nwra.com

waves reach the critical line the potential vorticity contours overturn in the horizontal, and deform the region of $f(f-u_y)<0$. This has the effect of locally increasing the meridional extent of the inertially unstable region at some longitudes and locally decreasing this extent at others. This asymmetry in the region of EQII triggers the instability so that the number of regions of instability are determined by the winter planetary wave forcing.

It should be noted that the planetary waves also set up a cross-equatorial flow towards the north pole which contributes to the maintenance of a nonzero shear at the equator.

2.3 Structure of EQII

The zonally averaged response in the tropical stratosphere in the meridional wind $\bar{v}$ is shown in Figure 2. The exact time and location that the EQII first appears depends on the initial zonal wind shear and the strength of the planetary wave forcing. The initial response is as expected from linear theory, with gridscale stacked-pancake structures in $\bar{v}$. Later in the run, the response develops a deeper vertical wavelength, consistent with zonally symmetric, nonlinear theory (Griffiths 2003). By this time the region of EQII has decreased in size, although still persists at higher altitudes very close to the equator.

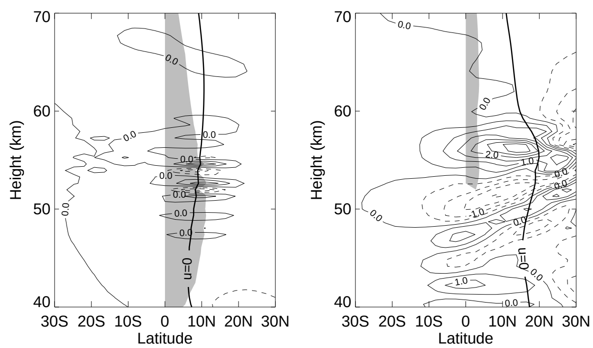

Figure 2: Zonal-mean meridional velocity for day 35 (left panel) and day 55 (right panel). Contour intervals are $0.5\,\mathrm{m\,s^{-1}}$. The $\bar{u}=0$ line is indicated by the thick line and region of EQII is shaded.

The structure of the EQII in the zonal-height cross-section is shown in Figure 3 for days 40 and 60 at 5.5°N. The disturbances are clearly limited to the altitudes between 45km and 60km, and occur at two equally spaced longitudes (due to the zonal wavenumber 2 planetary wave forcing). The region of EQII is destroyed level by level and first disappears where the instability is largest, at ~ 55km. This is also near the level where the $\bar{u}=0$ line enters the region of instability, and where the region of EQII is broadest.

Later in the run, the region of EQII at 5.5°N has been destroyed, although regions of $f(f-u_y)<0$ still remain. The gridscale structures from day 40 have developed a deeper wavelength. More interesting are the relatively small-scale waves that appear to eminate from the region of instability. These waves have a positive phase tilt with height, suggestive of upward propagating gravity waves, and their amplitude increases with height. Regions of Kelvin-Helmholtz instability, where the Richardson number $Ri = N^2/\bar{u}_z^2 < \frac{1}{4}$, occur in these areas, although it is unclear whether the waves, which produce a strong vertical shear, produced these regions, or these regions produce the waves.

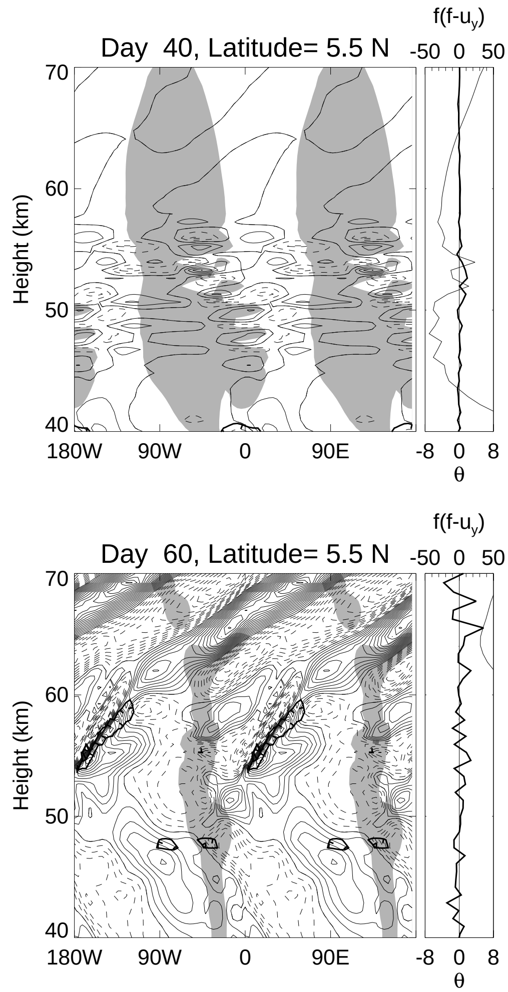

Figure 3: The temperature perturbation at 5.5°N for day 40 (upper set of panels) and day 60 (lower set of panels) with contour interval 2K. Negative contours are dashed. Values of local $f(f-u_y)<0$ are shaded and regions where the Richardson number Ri $<\frac{1}{4}$ are indicated by the thick line (most notable for day 60 at 55-60 km and 180°W and 0). The side panel shows the zonal-mean temperature perturbation at 5.5°N (thick line, bottom axis) and $f(f-\bar{u}_y)<0$ scaled by Earth's radius in units of $\mathrm{m\,s^{-1}days^{-1}}$ (thin line, top axis).

The rearrangement of absolute angular momentum $\bar{M}$ produces a region of negative meridional potential vorticity gradient $\partial\bar{P}/\partial\varphi$ on the summer side of the equator. This region, which extends vertically from $\sim 50-60$km is barotropically or baroclinically unstable (see Figure 4). The development of this region is important since it allows for the generation of a two-day wave through barotropic instability (Limpasuvan et al. 2000).

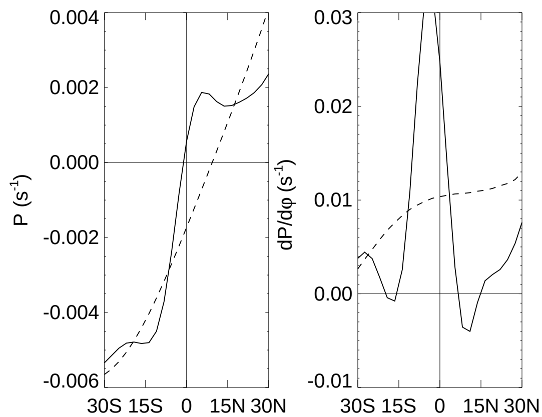

Figure 4: The zonal-mean profiles at 55km for potential vorticity (left panel) and the meridional gradient of potential vorticity (right panel) for day 0 (dotted line) and day 75 (solid line).

2.4 *Gravity wave generation*

Positive Eliassen-Palm flux divergences (not shown) of the tropical stratopause region suggest that this is a region of wave generation. A spectral analysis on the potential temperature in (x,z,t)-space is performed to determine the characteristics of these waves. The anaylsis in z is perfomed between 30km and 70km since the EQII response is limited to these altitudes. A density factor of $e^{z/H}$ was assumed in the model data and removed before the Fourier decomposition was performed. The analysis in time is performed using a 3 hour sampling rate and an 8 day sliding window, in order to allow wave amplitudes to change with time.

In the case shown here, the forced planetary wave is zonal wavenumber 2, and all other waves are higher harmonics of the original planetary wave (only even zonal wavenumbers have nonzero power). Shown in Figures 5 and 6 are the power spectra in $\omega - m$ for both zonal wavenumbers 10 and 20, although other wavenumbers shown very similar results. Runs with zonal wavenumber 1 planetary wave forcing produce all gravity waves of all zonal wavenumbers 1-42.

The dispersion relations for hydrostatic gravity and inertio-gravity waves are as follows

$$\hat{\omega}_{gw} = \mp \frac{Nk}{\hat{m}}, \qquad \text{and} \qquad \hat{\omega}^2_{igw} = \sqrt{f^2 + \frac{N^2k^2}{\hat{m}^2}} \qquad (2)$$

where $\hat{\omega} = \omega - \bar{u}k$ is the doppler shifted frequency, and $\hat{m}^2 = m^2 + 1/4H^2$ is the vertical wavenumber including the shift due to density. The dispersion relations for both the upward and downward propagating gravity waves are plotting in Figures 5 and 6 since it is conceivable that both

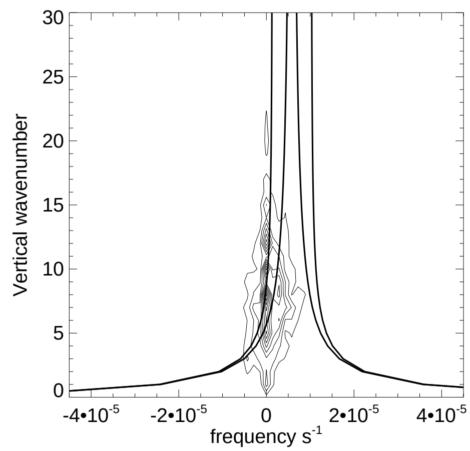

Figure 5: The spectral decomposition of θ at 10°N, day 65 and for zonal wavenumber 10. The dispersion relations for upward and downward propagating gravity and inertio-gravity waves are indicated by the thick lines. (From left to right, the thick lines represent the dispersion relations for upward propagating inertio-gravity waves, upward propagating gravity waves, downward propagating gravity waves and downward propagating inertio-gravity waves.

waves may be generated by the EQII. The power spectra strongly suggest that the waves generated by the EQII are upward propagating gravity waves or inertio-gravity waves, although it is difficult to distinguish between the two with these data.

3 DISCUSSION

The EQII was studied using a primitive equations model and allowing the instability to have a zonal structure. The zonal-mean structure of the EQII generated here compares well with other studies, both linear and nonlinear, that use zonally symmetric models. The initial vertical

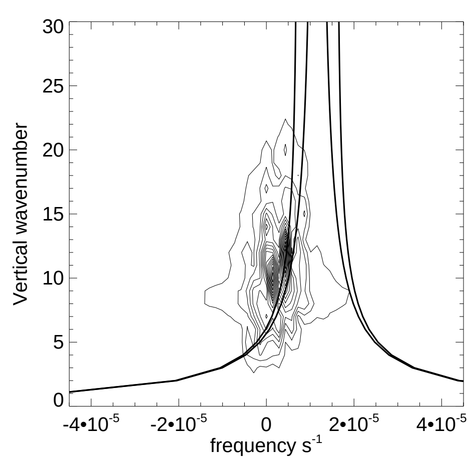

Figure 6: As for Figure 5 but for zonal wavenumber 20.

structure is gridscale, and as the EQII develops in time, evolving to a more nonlinear state, the vertical wavelength deepens.

Different forced planetary waves from the winter hemisphere produce slightly different results. If only zonal wavenumber one is used, the instability that develops is wavenumber one, but gravity waves of all zonal wavenumbers are generated. Also, it appears that a zonal wavenumber 1 instability is less effective at redistributing $\bar{M}$ to a stable state. If both wavenumbers 1 and 2 are used, the resulting instability is primarily wavenumber 1 with a smaller wavenumber 2 component. A stronger initial meridional shear in $\bar{u}$ results in a more extensive region of inertial instability, and a stronger response earlier in the run. Regions of $Ri < \frac{1}{4}$ are also more readily produced.

An important consequence of EQII is gravity wave or inertio-gravity wave generation in the tropical stratopause region. Gravity waves are important in the middle atmosphere since their dissipation in the mesosphere is responsible for the global circulation from summer pole to winter pole at these altitudes. In this case, the gravity waves generated are close to stationary waves and appear to have some propagation away from the tropics. Thus, these waves could also be responsible for helping to maintain the shear zone at the top of the middle atmospheric jets (although there are certainly other sources of gravity waves). The shear at the top of the summer hemisphere jet may be the source of the two-day wave generated as a baroclinic instability (Norton and Thuburn 1996; Salby and Callaghan 2001). In addition to the creation of the the region of negative potential vorticity gradient in the summer tropics, it seems that EQII may be very important for understanding the two-day wave in the mesosphere.

REFERENCES

Andrews, D. G., J. R. Holton, and C. B. Leovy (1987). *Middle Atmosphere Dynamics*, Volume 40 of *International Geophysical Series*, Chapter 3, pp. 114. Academic Press, Inc.

Clark, P. D. and P. H. Haynes (1996). Inertial instability on an asymmetric low-latitude flow. *Quart. J. Roy. Meteor. Soc. 122*, 151–182.

Dunkerton, T. J. (1981). On the inertial stability of the equatorial middle atmosphere. *J. Atmos. Sci. 38*, 2354–2364.

Dunkerton, T. J. (1993). Inertial instability of nonparallel flow on an equatorial β plane. *J. Atmos. Sci. 50*, 2744–2758.

Griffiths, S. J. (2003). Nonlinear vertical scale selection in equatorial inertial instability. *J. Atmos. Sci. 60*, 977–990.

Hayashi, H., M. Shiotani, and J. C. Gille (1998). Vertically stacked temperture disturbances near the equatorial stratopause as in seen in Cryogenic Limb Array Etalon Spectrometer data. *J. Geophys. Res. 103*, 19 469–19 483.

Limpasuvan, V., C. B. Leovy, Y. J. Orsolini, and B. A. Boville (2000). A numerical simulation of the two-day wave near the stratopause. *J. Atmos. Sci. 57*, 1702–1717.

Norton, W. A. and J. Thuburn (1996). The two-day wave in a middle atmosphere GCM. *Geophys. Res. Lett. 23*, 2113–2116.

O'Sullivan, D. J. and M. H. Hitchman (1992). Inertial instability and Rossby wave breaking in a numerical model. *J. Atmos. Sci. 49*, 991–1002.

Salby, M. L. and P. F. Callaghan (2001). Seasonal amplification of the 2-day wave: Relationship between normal mode and instability. *J. Atmos. Sci. 58*, 1858–1869.